Solar Phys (2010) 266: 109–121
DOI 10.1007/s11207-010-9596-2

Gyrosynchrotron Emission from Anisotropic Pitch-Angle Distribution of Electrons in 3-D Solar Flare Sources

P.J.A. Simões · J.E.R. Costa

Received: 9 February 2010 / Accepted: 21 June 2010 / Published online: 22 July 2010

Abstract We present calculations, made for the first time, of the gyrosynchrotron emission by mildly relativistic electrons with anisotropic pitch-angle distribution using a realistic magnetic loop model in three dimensions. We investigated the intensity, spectral index of the optically thin region of the spectrum, the spatial morphology and the dependency on the source position on the solar disk. The method to describe a three-dimensional source and the procedure to perform the calculations are presented. We have modified the Ramaty's gyrosynchrotron code to allow the evaluation of anisotropic pitch-angle electron distributions, as described in the complete formalism. We found that anisotropic electron distributions affect the intensity of the radiation, spatial morphology and spectrum of spatially resolved sources. However, the spatially integrated spectrum of the emission seems to be insensitive to the electron pitch-angle distribution, as the magnetic field inhomogeneity smooths out the effects of the anisotropic distribution in the produced radiation, in contrast to homogeneous sources.

Keywords Flares: models · Flares: relation to magnetic field · Flares: spectrum · Radio bursts: microwave (mm, cm)

1. Introduction

The microwave spectrum of solar flares is believed to be produced by gyrosynchrotron emission from non-thermal electrons trapped in magnetic loops. The radiation is produced by the interactions of the accelerated electrons with the magnetic field and background ambient plasma. The efficiency and the characteristics of the radiation are affected by the parameters

P.J.A. Simões (✉)
Centro de Rádio Astronomia e Astrofísica Mackenzie – CRAAM, Rua da Consolação, 896, São Paulo, 01302-907 SP, Brazil
e-mail: paulo@craam.mackenzie.br

J.E.R. Costa
Instituto Nacional de Pesquisas Espaciais – INPE, Av. dos Astronautas, 1.758, São José dos Campos, 12227-010 SP, Brazil
e-mail: jercosta@das.inpe.br

of the non-thermal electrons, such as energy distribution, pitch-angle distribution and number density, and also by the source parameters, as magnetic field strength and geometry, and ambient plasma density (see Bastian, Benz, and Gary, 1998 for a review of radio emission of solar flares). Although the complex structure of solar flare sources had been suggested by several authors in the literature and have been confirmed by EUV images of the coronal magnetic loops, the vast majority of flare analyses were done based on homogeneous source parameters. On the other hand, several authors had shown the characteristics of gyrosynchrotron emission from inhomogeneous sources through models, with some applied to observations. Alissandrakis and Preka-Papadema (1984) have shown the effect of magnetic field geometry on the morphology of intensity and polarization using a bidimensional dipole magnetic field model. Klein and Trottet (1984) and Lee, Gary, and Zirin (1994) followed the approach to calculate the effect not only on morphology but on the spectrum, and Simões and Costa (2006) improved the Alissandrakis and Preka-Papadema (1984) approach by using a set of 3-D magnetic arcs to study the radiation intensity, spectrum and spatial morphology. Nindos *et al.* (2000) and Kundu *et al.* (2001) applied a simple arc geometry to represent the magnetic structure of a flaring loop in studying the intensity variation of the emission along the loop.

Many theoretical models have suggested the possibility of anisotropic pitch-angle distributions of accelerated electrons (see, *e.g.*, Pryadko and Petrosian, 1999). Nevertheless, in flare analyses, the electron distribution is generally referred to by an energy power-law with an isotropic pitch-angle distribution. This common assumption evidences the difficulties in evaluating the initial electron pitch-angle distribution and its time evolution. The importance of the pitch-angle distribution was investigated in several works (Wu and Lee, 1979; Melrose, Hewitt, and Ronnmark, 1982; Sharma and Vlahos, 1984; Aschwanden and Benz, 1988; Fleishman and Yastrebov, 1994; Ledenev, 1998; Vlasov, Kuznetsov, and Altyntsev, 2002; Fleishman and Melnikov, 2003b). However, most of them focused in the optically thick region of the spectrum, studying the conditions for the occurrence of negative self-absorption, and thus an electron cyclotron maser. Investigating the whole gyrosynchrotron spectrum, Fleishman and Melnikov (2003a) showed that highly anisotropic distributions can considerably affect the microwave spectrum produced in homogeneous sources. The emission intensity can change up to a few orders of magnitude the optically thin region of the spectrum, compared with the isotropic case, thus significantly affecting the spectral index.

Dulk and Marsh (1982) have found that the optically thin spectral index α can be linked to the energy power-law index δ of electrons in the isotropic pitch-angle distribution by the relation

$$\alpha = 0.90\delta - 1.22. \tag{1}$$

If the electrons have an anisotropic pitch-angle distribution, this relation may need to be modified. Fleishman and Melnikov (2003a) also mention that this method cannot be applied directly if the radiating electrons have an anisotropic pitch-angle distribution since the spectral index deviates significantly from the respective value for the isotropic case.

Lee and Gary (2000) showed that an initial anisotropic electron distribution is necessary to explain the spectral evolution observed by Lee, Gary, and Shibasaki (2000). They studied the kinetics of electrons, considering magnetic mirroring and weak Coulomb scattering, in a particular microwave burst. The pitch-angle distribution evolution in time was evaluated, and the microwave spectrum computed. The spectral evolution is only explained considering an initial anisotropic pitch-angle distribution. Lee and Gary (2000) also note that the initial pitch-angle distribution can provide important information to investigate the acceleration mechanism.

Our main interest here is to analyze the effects of an anisotropic pitch-angle distribution of electrons on the gyrosynchrotron radiation. Such calculations have thus far been made only for homogeneous sources and this is the first time for anyone to investigate the effects using an inhomogeneous magnetic loop model in 3-D. We then compare with the emission characteristics of isotropic distribution of electrons, presented in Simões and Costa (2006). In Section 2 we describe the method to represent a three-dimensional burst source and the procedure of calculations of the emission. The numerical results are presented and analyzed in Section 3. In Section 4, we discuss our results.

2. Description of the Method

Our method to calculate gyrosynchrotron emission produced in 3-D sources may be divided in three steps: description of the flare environment (magnetic field and ambient plasma density); calculation of emission and self-absorption coefficients; evaluation of the radiative transfer through the source. We presented this method in a previous paper to evaluate the effects of the source geometry in the produced microwave radiation (Simões and Costa, 2006), and it is summarized here.

2.1. Environment

To represent inhomogeneous sources, we define a three-dimensional discrete space, in which a set of voxels (volume elements) defines the magnetic geometry. Each voxel is considered as a homogeneous source with singly assigned values of magnetic field strength and ambient density. The locations of the voxels are specified in Cartesian coordinates (i, j, k). The spatial structure of the set of voxels constitutes an inhomogeneous source, with spatial variation in both magnetic field and ambient density. It is important to note that this geometric description of the magnetic field does not imply a specific technique to obtain the direction and induction of the field. Thus, a force-free field extrapolation (see, *e.g.*, Sakurai, 1981) or tomographic reconstruction (see, *e.g.*, Wiegelmann and Inhester, 2003; Simões and Costa, 2003) methods can be applied. The ambient density is also defined as an input parameter, and it can be modeled as an hydrostatic equilibrium atmosphere, or any other atmospheric density model desired. The viewing angle θ of the magnetic field at each voxel is found from the scalar product of the magnetic field vector and the z-axis taken as the line of sight.

The adopted geometry of the magnetic field for this work is an idealized set of 30 semi-circular arcs that are created by randomly varying the height in the range $1-2\times10^9$ cm, inclination angle in the range $\pm5^\circ$ with respect to the local vertical line, and azimuth angle in the range $\pm5^\circ$. This results in a magnetic field configuration similar to that of typical EUV loops. This configuration is shown in Figure 1.

The magnetic field strength B for this structure was calculated using a simple dipole approximation. The dipole parameters were chosen to set the magnetic field strength about 1000 G (gauss) at the magnetic loop feet and 100 G at the loop top.

As also noted in Simões and Costa (2006), our intention was not to model a specific magnetic field region, but to investigate the general effect of 3-D magnetic field structure on the flare emission. Force-free field (linear or non-linear) extrapolations may be used when studying a specific flare, even to test if the extrapolation method can successfully describe the magnetic field under flare conditions.

The ambient plasma density N was calculated using an exponential function with height h:

$$N(h) = N_0 \mathrm{e}^{-\frac{h}{H}} \tag{2}$$

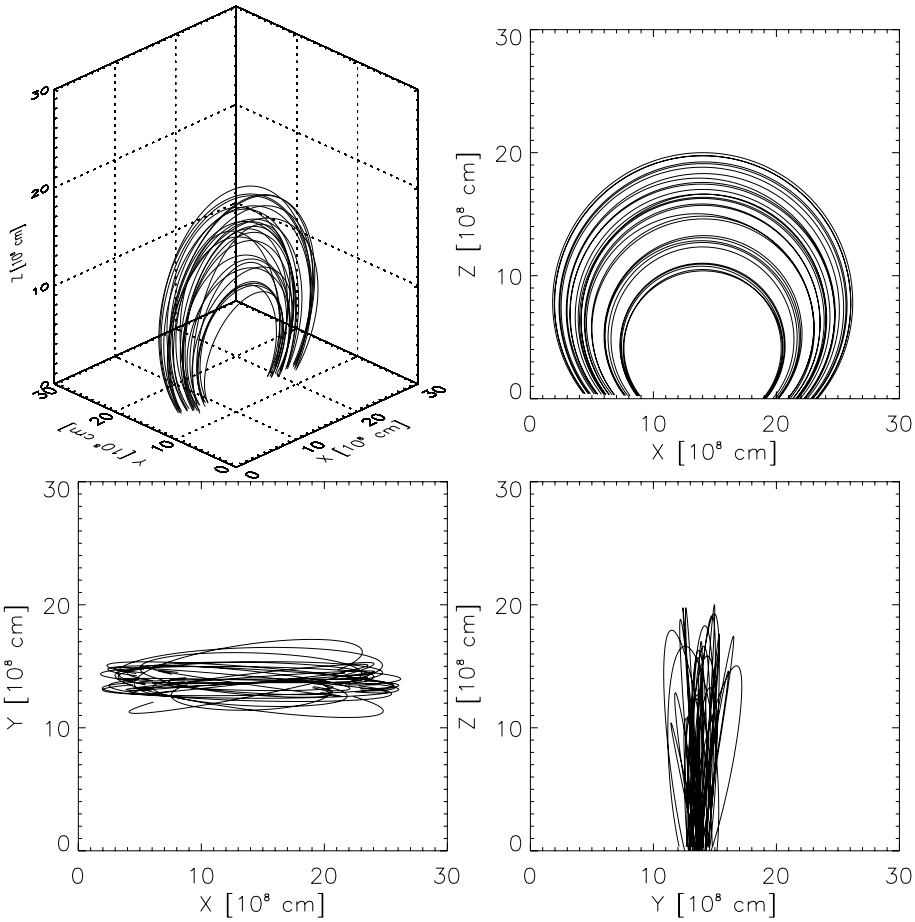

Figure 1 The adopted three-dimensional magnetic field structure: perspective view and three orthogonal projections.

where $N_0 = 1 \times 10^{11}$ cm^{-3} is the density at the bottom layer of the source volume and $H = 5 \times 10^8$ cm is the scale height. Usually, the scale height is treated as a function of the temperature, as in Aschwanden *et al.* (1999); however, in this work, the ambient density profile was set to avoid Razin suppression, so that we can focus on the effect of the pitch-angle distribution on the gyrosynchrotron spectrum. Depending on the ambient plasma density and magnetic field strength, and electron energy, the Razin effect suppresses the radiation, usually in lower frequencies (see Ramaty, 1969).

Once the source parameters (magnetic field strength – B and θ – and ambient density N) that control the gyrosynchrotron emission are specified in the discrete space in Cartesian coordinates (i, j, k), the emission and self-absorption coefficients can be computed.

2.2. Calculations of Emission and Self-Absorption Coefficients

The complete formalism to calculate the gyrosynchrotron radiation produced in homogeneous sources was presented by Ramaty (1969). Since in our method each voxel is a ho-

mogeneous source, we have used Ramaty's code (Ramaty, 1969; Ramaty *et al.*, 1994) to calculate the emission j_ν and self-absorption κ_ν coefficients, for both the ordinary and extraordinary magneto-ionic modes. We have modified Ramaty's code to include the complete expressions for j_ν and κ_ν (given in Ramaty, 1969), allowing for the evaluation of anisotropic pitch-angle distributions.

The coefficients are calculated by numerical integration, using the Gauss–Legendre method. Bessel functions are calculated using the IDL BESELJ function, and recursive relations for the derivatives. We assume a cold and collisionless plasma permeated by a static and uniform (in each voxel) magnetic field.

2.2.1. Electron Distribution Function

The momentum distribution function of the non-thermal electrons may be separated into an energy distribution $u(E)$ and a pitch-angle distribution $g(\phi)$ (Ramaty, 1969). The energy spectrum of non-thermal electrons is usually described as a power-law function:

$$N_\mathrm{e} = \int_{E_\mathrm{min}}^{\infty} u(E)\,\mathrm{d}E = \int_{E_\mathrm{min}}^{\infty} E^{-\delta}\,\mathrm{d}E \tag{3}$$

where E_min is the energy lower limit. In numerical approaches, the upper limit of the integral is usually replaced for a practical limit by E_max. In all our calculations, we set these limits as $E_\mathrm{min} = 10$ keV and $E_\mathrm{max} = 100$ MeV to avoid the effects of low and high energy cutoffs in the resulting spectra (Holman, 2003). We used a typical value for the energy spectral index, $\delta = 3$ (Alissandrakis, 1986; Staehli, Gary, and Hurford, 1989; Lim *et al.*, 1992; Silva, Wang, and Gary, 2000), and $N_\mathrm{e} = 6 \times 10^7$ cm^{-3} for the non-thermal electron density. We assumed a homogeneous density of the non-thermal electrons along the magnetic arcs. This electron energy spectrum and the source model are the same as we investigated in Simões and Costa (2006), so we can compare the results from isotropic and anisotropic electron distributions in the 3-D source.

We represented the pitch-angle distribution as a sine function (Ramaty, 1969; Fleishman and Melnikov, 2003a):

$$g(\phi) = \frac{1}{4\pi} \sin^m \phi \tag{4}$$

where the power m indicates the anisotropy of the distribution, and ϕ is the pitch-angle value. An isotropic distribution is obtained with $m = 0$, while higher values of m represents higher anisotropic distributions. Here, we used $m = 10$, giving $g(70°)/g(90°) = 0.5$.

As each homogeneous voxel has a different magnetic field strength **B** and ambient density N, the source will have different spatial characteristics of emission and absorption.

2.3. Radiative Transfer

The frequency spectrum (I_ν) of gyrosynchrotron emission produced by an electron distribution with a power-law energy spectrum typically shows an optically thick part, with I_ν rising with frequency, and an optically thin part, I_ν falling with frequency. In an analysis based on homogeneous source models, it is usually assumed that the spectral maximum occurs at a frequency where $\tau \approx 1$, where τ is the optical depth of the source. When considering 3D source models, this considerations may not be correct, since the magnetic field geometry might affect the observed spectrum (Simões and Costa, 2006).

Our method to solve the radiative transfer equation is based on the assumption that the voxels are homogeneous regions, thus we can use the analytical solution for the radiative transfer equation. We also assume that the ray paths are straight lines, since the refraction index varies slowly in space and its value is close to unity, for microwave wavelengths. The voxel-volume where the field lines are defined is rotated and the coordinate system is redefined, with the z-axis aligned with the line of sight; thus, the magnetic structure becomes oriented as viewed by the observer. Once all the coefficients are calculated by our modified Ramaty's code, these values are associated with their respective voxel (i, j, k). The analytical solution for the radiative transfer in a homogeneous source is given by

$$I_{\nu_s} = \frac{j_{\nu_s}}{\kappa_{\nu_s}}\left(1 - \mathrm{e}^{-\kappa_{\nu_s} l}\right), \tag{5}$$

where I_{ν_s} is the radiation produced in the sth voxel (the index s indicates the voxel number in the line of sight, from the farthest to the nearest layer of voxels) and l is the voxel depth. This specific intensity becomes the input of the next voxel according to

$$I_{\nu_{s+1}} = I_{\nu_s}\mathrm{e}^{-\kappa_{\nu_{s+1}} l} + \frac{j_{\nu_{s+1}}}{\kappa_{\nu_{s+1}}}\left(1 - \mathrm{e}^{-\kappa_{\nu_{s+1}} l}\right). \tag{6}$$

This proceeds until the end of the source, *i.e.* the nearest layer to the observer, thus the intensity at each map pixel is obtained by integration of the radiative transfer equation along a column of voxels. The flux density is then obtained by

$$F_\nu = I_\nu \Delta\Omega, \tag{7}$$

where $\Delta\Omega$ is the pixel solid angle. By repeating this procedure over the entire source, we obtain a two-dimensional map of flux density. The flux of the whole source can be easily obtained by summing up the flux densities in all pixels. This procedure is applied independently for the ordinary and extraordinary wave modes. The total flux and polarization maps are obtained by the sum and difference of the extraordinary and ordinary emission maps, respectively.

2.4. Source Position

In order to examine the geometric effects of the source in the emission produced, we computed the gyrosynchrotron emission in the previously described source positioned in three different locations on the solar disk: S20W0 (center), S20W40, and S20W80 (near limb), as shown in Figure 2.

3. Numerical Results and Discussion

Using the method described, we computed the gyrosynchrotron radiation produced by non-thermal electrons with both anisotropic and isotropic pitch-angle distributions (Simões and Costa, 2006) in an idealized three-dimensional source configuration. In order to verify the characteristics of the emission in this proposed environment, the resulting spectra were compared with the characteristics of the emission from anisotropic pitch-angle electrons in homogeneous sources. The parameters chosen for this calculations were: viewing angles θ ranging from 10° to 80°, in 10° steps, anisotropic pitch-angle distribution

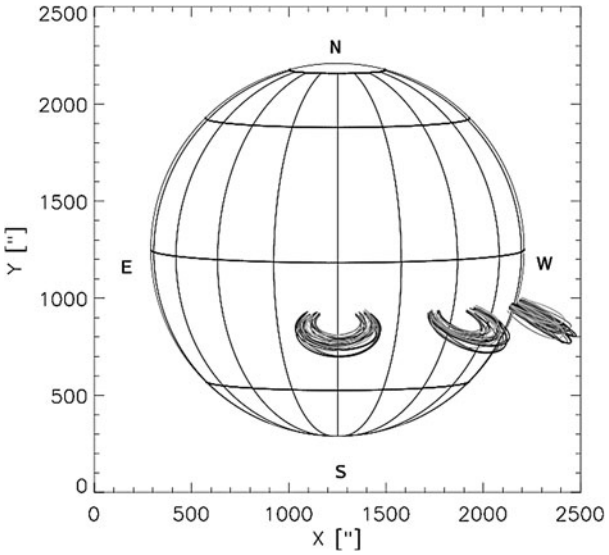

Figure 2 Source heliographic positions: S20W0 (center), S20W40 and S20W80 (near limb). The arcs are enlarged by a factor of 15 to make them better visible.

$g(\phi) = (1/4\pi)\sin^{10}\phi$, energy spectral index $\delta = 3$, magnetic field $B = 500$ G, energy range $E_{\rm min} - E_{\rm max} = 10$ keV – 100 MeV, non-thermal electron density $N_{\rm e} = 6 \times 10^7$ cm^{-3}, source depth $l = 10^9$ cm, source solid angle $\Omega = 13''$ and Razin parameter $\alpha_{\rm R} = 3$ (Ramaty, 1969). The Razin parameter is defined as $\alpha_{\rm R} = 1.5\nu_B/\nu_{\rm p}$, where ν_B is the gyrofrequency and $\nu_{\rm p}$ is the plasma frequency. In Section 3.1 we will discuss the spatially integrated flux spectrum, while the spatially resolved flux spectrum will be discussed in Section 3.3.

3.1. Spectral Characteristics

3.1.1. Homogeneous Case

As shown by Fleishman and Melnikov (2003a), the radiation produced by anisotropic electrons presents changes in intensity, polarization and spectral index, compared to the radiation produced by an isotropic distribution. The most important information revealed by these authors is the significant change in the optically thin spectral index of the spectrum. The reasons may be summarized as follows: the synchrotron emission produced by a single electron is radiated in a narrow cone with width of $\vartheta \approx \gamma^{-1} = mc^2/E$, along the electron velocity, where γ is the Lorentz factor, E is the electron energy, m is the electron mass and c is the speed of light. Thus, in a constant magnetic field, high energy electrons produce beamed high frequency radiation, while low energy electrons produce low frequency radiation in a wide cone. From this analysis, if the line of sight of the observer coincides with the direction in which the electron pitch-angle distribution is maximal, the observer will detect the emission from low and high energy electrons, resulting in a spectrum almost identical with the spectrum produced by an isotropic distribution. On the other hand, if the line of sight is outside the cone of maximum anisotropy, only the emission from low energy electrons will be detected, since their radiation pattern is almost omnidirectional. This scenario will provide a much softer spectral index.

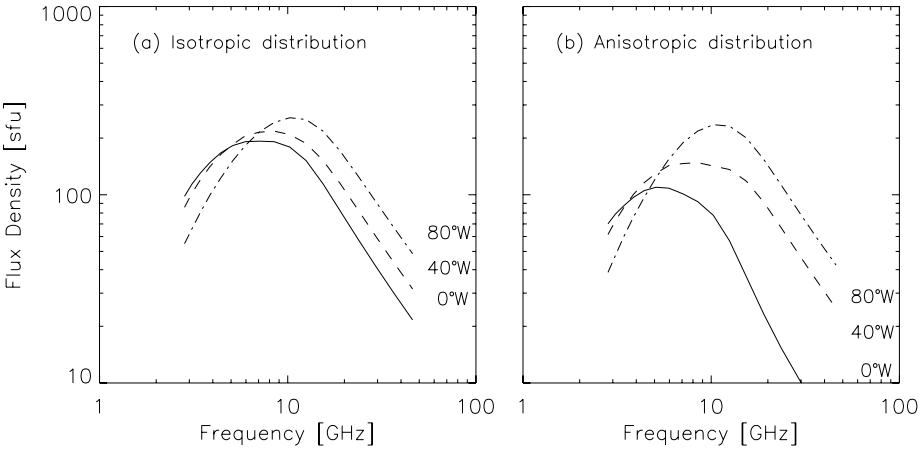

Figure 3 Calculated spectra for our source model at three solar longitudes: 0°W (continuous), 40°W (dashed), and 80°W (dash-dotted). Panel (a) is for isotropic and panel (b) is for anisotropic pitch-angle distributions, respectively.

Figure 4 Optically thin spectral index α as a function of viewing angle. Diamonds, crosses and asterisks are for isotropic, anisotropic, and homogeneous cases, respectively.

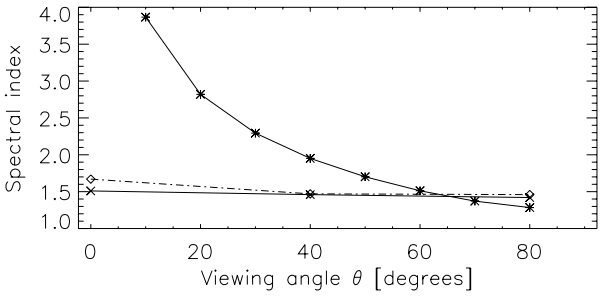

3.1.2. Inhomogeneous Case

The optically thin spectral index α is commonly linked to the energy spectral index δ of the radiating electrons directly (Equation (1)). Fleishman and Melnikov (2003a) showed that one must be careful when using this assumption, since the anisotropy changes the spectral index significantly, as noted earlier. However, as we show here, when considering a more realistic source structure, as magnetic loops, the geometry of the magnetic field smooths out the effect of directivity created by the anisotropy and the beaming radiation of the high energy electrons. Thus, the spectral index of the emission from an anisotropic distribution is very similar to the spectrum produced by an isotropic distribution, as can be seen in Figures 3 and 4. In homogeneous sources, the spectral index varies from -1.3 to -3.8 (varying the viewing angle from 10° to 80°), while in the loop source, its value is practically constant (see Table 1). Moreover, using Equation (1) with our resulting spectral index values, we find values of the energy spectral index δ very close to the value input in the calculations ($\delta = 3$). These values are presented in Table 1.

Table 1 Optically thin spectral index α from our 3D loop sources and energy spectral index δ, obtained from Equation (1).

Isotropic	α	δ	Anisotropic	α	δ
0°W	−1.51	−3.04	0°W	−1.67	−3.21
40°W	−1.46	−2.98	40°W	−1.47	−2.99
80°W	−1.42	−2.94	80°W	−1.46	−2.98

3.2. Spatial Characteristics

From the procedure described in Section 2, we calculated maps of the gyrosynchrotron emission from the three-dimensional loop source. Some of these maps, at 3 GHz and 10 GHz, calculated for anisotropic and isotropic distributions, are presented in Figure 5. Our calculated emission maps show the same main features as those commonly seen in spatially resolved observations and predicted by previous models (Alissandrakis and Preka-Papadema, 1984; Klein and Trottet, 1984; Simões and Costa, 2006): lower frequencies reveal extended sources, associated with looptop emission, and the higher frequencies revealed one or two compact emitting sources associated with footpoints. This common characteristic can easily be explained by the intensity of the magnetic field in each part of the loop: weak magnetic field strength in the looptop and strong magnetic field strength on footpoints. An interesting result here is the presence of a third kernel, at the high frequency maps on the center of the solar disk, associated with the looptop (Figure 5, top-left frame). The feature is not present in the isotropic distribution maps (top-right frame), evidencing the effect of the anisotropy. This looptop source in the 10 GHz map, which also appears at higher frequencies, is revealed due to the high directivity of the electron radiation pattern. In the isotropic case this does not happen, because the footpoint sources are much stronger than the emission of the looptop, obscuring it. From the limb sources (bottom row frames of Figure 5), we can see that the position of the 3 GHz and 10 GHz sources are slightly modified by the pitch-angle anisotropy, but, from morphology alone, there are no clear signs that could reveal the existence of an anisotropic distribution. For the adopted geometry, the looptop source (3 GHz) is mainly produced by a low energy electron, which has no directivity, while the high energy electron that produces the footpoint source (10 GHz) is pointed to the observer due to its pitch-angle anisotropy. Thus, the spatial morphology resembles that of an isotropic case.

3.3. Characteristics of Spatially Resolved Spectrum

We also analyzed the spectrum of spatially resolved regions of the source. We selected two square regions, one at the looptop and one at the one footpoint. The size of each square region is $10'' \times 10''$ (40×40 pixels). The resulting spectra for looptop and footpoint are shown in Figure 6, for the source positioned at the center and in the limb of the solar disk. In both cases, the looptop spectrum peaks at a lower frequency than the footpoint spectrum, evidencing different effective magnetic field strengths in each region. The analysis of the spectral slopes requires some discussion. The frequency peak and spectral index values for the center disk source are shown in Table 2.

For the center disk source (Figure 6(a)), the anisotropic effects have a low efficiency to shape the spectrum at lower frequencies, and the weak emission of high frequency radiation from the looptop results in similar spectra for both isotropic and anisotropic

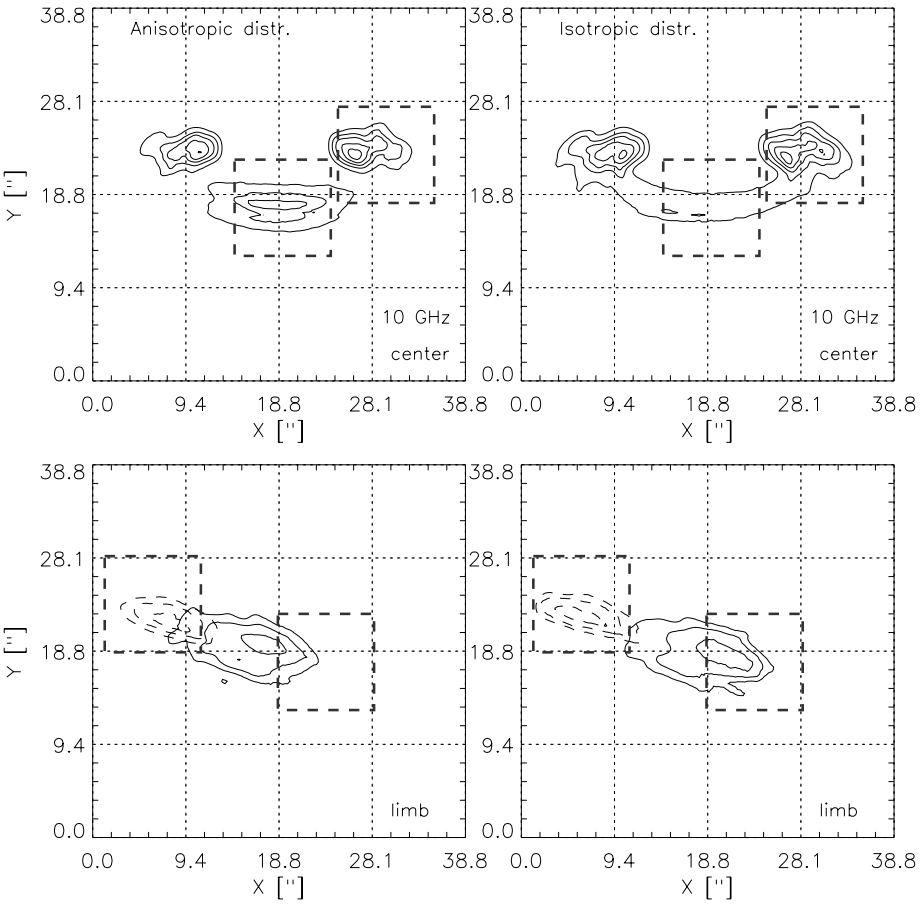

Figure 5 Flux density maps calculated for center (top row) and limb (bottom row) sources. Left column: Anisotropic case. Right column: Isotropic case. The contour levels are 10, 30, 50, 70, and 90% of normalized flux in the top frames, and 50, 70 and 90% in the bottom frames. At the bottom frames, 3 GHz emission is represented by continuous contours and 10 GHz emission by dashed contours. The $10'' \times 10''$ dashed lined boxes indicate the regions taken to simulate high spatial resolution spectra. In these maps, the north is up and west is to the right.

cases. However, in the footpoints, viewed in a quasi-longitudinal direction, the beaming radiation effects of the high energy electrons is very significant to shape the spectrum. The emission of these electrons is not pointed to the observer, and this effect becomes more effective with increasing electron energy, making the spectral slope softer than the looptop spectrum, and also softer than the integrated spectrum. This is interesting because when considering sufficiently small regions, the main characteristics of the emission from an anisotropic pitch-angle distribution (as detailed by Fleishman and Melnikov, 2003a) are present; hence the region can be considered as slightly homogeneous. Moreover, different spectral slopes for separated regions of a flaring source have been verified in spatially resolved observations (Wang *et al.*, 1994; Lim *et al.*, 1994; Yokoyama *et al.*, 2002).

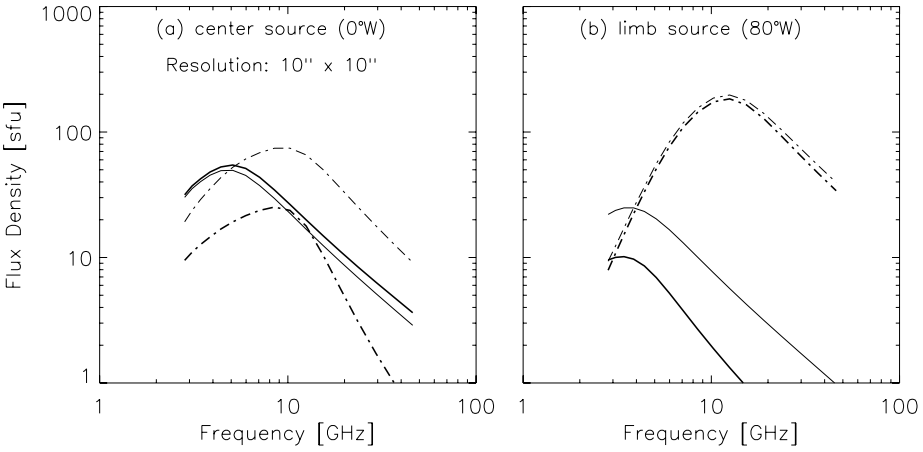

Figure 6 Looptop (continuous lines) and footpoint (dash-dotted) spectra for the isotropic (thin lines) and anisotropic (thick) pitch-angle distributions, at (a) center and (b) limb positions.

Table 2 Peak frequency and spectral index values for the looptop and footpoint of the source at the center of the solar disk (Figure 6).

	Looptop		Footpoint	
	ν_{peak}	α	ν_{peak}	α
Isotropic	4.8 GHz	−1.3	8.8 GHz	−1.5
Anisotropic	4.8 GHz	−2.4	8.8 GHz	−1.3

In the limb source (Figure 6(b)), the spectral indexes of both regions of the loop are very close to the value of the spectral slope of the spatially integrated spectrum ($\alpha = -1.4$). In the looptop source, the directivity is low, because of the wide cone of radiation of the low energy electrons, and the emission of higher frequencies is not efficient (because of the low magnetic field strength in the region); thus, the spectrum shape is very similar compared to the isotropic case. The footpoint source is viewed in a quasi-transversal angle, making the effects of the anisotropy undetectable to the observer, thus this spectrum is almost identical to the isotropic case.

In the optically thin regime, the spectral index is only dependent on the electrons' distribution function (in energy and pitch-angle); thus, different spectral indexes from different regions of the same source may suggest the presence of anisotropy in the pitch-angle distribution, especially if it is possible to infer the loop geometry from the EUV data, for example. However, the current difficulties inferring the loop geometry from observational data may leave ambiguity in identifying such anisotropic features. It is worth noting that the local magnetic field strength and non-thermal electron density in those regions will just shift the spectrum peak in frequency (Staehli, Gary, and Hurford, 1989).

4. Summary

We presented the results of calculations of the gyrosynchrotron emission from a three-dimensional flaring loop, focused on the effects of anisotropic pitch-angle distributions of non-thermal electrons. The procedure of the computations used here were developed in Simões and Costa (2006) and summarized in this work.

Our calculations show that the overall shape of spatially integrated spectrum of a loop-like source filled with electrons in anisotropic pitch-angle distribution is not very different from that of an isotropic distribution. This property was not recognized in previous calculations of gyrosynchrotron radiation based on a homogeneous source model (see, *e.g.*, Fleishman and Melnikov, 2003a). Moreover, we have shown that the well-known expression presented by Dulk and Marsh (1982), which relates the optically thin spectral index with the energy spectral index of electrons (Equation (1)), can be applied successfully to estimate the energy distribution of the flaring electrons. It is important to mention that this method can only be used in a spatially integrated spectrum, since the pitch-angle anisotropy can change the spectral index of the spectrum of the resolved regions of the source.

Our results also show that anisotropic pitch-angle distributions of electrons affect the intensity, spatial morphology, and spectrum of spatially resolved sources of gyrosynchrotron emission. In our calculated maps, it is clear that anisotropic distributions can produce looptop sources at higher frequencies. This feature is highly dependent on the source geometry and the direction in which the electron pitch-angle distribution is maximal, since in the limb source, the looptop source is not present. This type of looptop source had been qualitatively explained as concentrations of electrons in this region due to a high anisotropic pitch-angle distribution and the effects of magnetic mirroring (Melnikov, Shibasaki, and Reznikova, 2002). Another typically observed characteristic of microwave is the combination of one large looptop source at lower frequencies and two compact footpoint of associated sources at higher frequencies. Such a morphology has been considered to be due to variation of the gyrosynchrotron opacity from the apex to footpoints of an inhomogeneous magnetic loop (see, *e.g.*, Alissandrakis and Preka-Papadema, 1984). Our calculations, employing both isotropic and anisotropic pitch-angle electron distributions, also reproduce this characteristic well and confirm the interpretation.

Acknowledgements We are deeply thankful to the anonymous reviewer for giving us clear statements and corrections improving the quality of the manuscript. We also thank Dr. C.G. Giménez de Castro for helpful suggestions and corrections on the manuscript. P.J.A. Simões also would like to thank FAPESP for supporting this work, under processes no. 03/03406-6 and no. 04/14248-5.

References

Alissandrakis, C.E.: 1986, *Solar Phys.* **104**, 207
Alissandrakis, C.E., Preka-Papadema, P.: 1984, *Astron. Astrophys.* **139**, 507
Aschwanden, M.J., Benz, A.O.: 1988, *Astrophys. J.* **332**, 447
Aschwanden, M.J., Newmark, J.S., Delaboudinière, J., Neupert, W.M., Klimchuk, J.A., Gary, G.A., Portier-Fozzani, F., Zucker, A.: 1999, *Astrophys. J.* **515**, 842
Bastian, T.S., Benz, A.O., Gary, D.E.: 1998, *Annu. Rev. Astron. Astrophys.* **36**, 131
Dulk, G.A., Marsh, K.A.: 1982, *Astrophys. J.* **259**, 350
Fleishman, G.D., Melnikov, V.F.: 2003a, *Astrophys. J.* **587**, 823
Fleishman, G.D., Melnikov, V.F.: 2003b, *Astrophys. J.* **584**, 1071
Fleishman, G.D., Yastrebov, S.G.: 1994, *Solar Phys.* **153**, 389
Holman, G.D.: 2003, *Astrophys. J.* **586**, 606
Klein, K.L., Trottet, G.: 1984, *Astron. Astrophys.* **141**, 67
Kundu, M.R., Nindos, A., White, S.M., Grechnev, V.V.: 2001, *Astrophys. J.* **557**, 880
Ledenev, V.G.: 1998, *Solar Phys.* **179**, 405
Lee, J., Gary, D.E.: 2000, *Astrophys. J.* **543**, 457
Lee, J.W., Gary, D.E., Zirin, H.: 1994, *Solar Phys.* **152**, 409
Lee, J., Gary, D.E., Shibasaki, K.: 2000, *Astrophys. J.* **531**, 1109
Lim, J., White, S.M., Kundu, M.R., Gary, D.E.: 1992, *Solar Phys.* **140**, 343
Lim, J., Gary, D.E., Hurford, G.J., Lemen, J.R.: 1994, *Astrophys. J.* **430**, 425
Melnikov, V.F., Shibasaki, K., Reznikova, V.E.: 2002, *Astrophys. J. Lett.* **580**, 185

Melrose, D.B., Hewitt, R.G., Ronnmark, K.G.: 1982, *J. Geophys. Res.* **87**, 5140
Nindos, A., White, S.M., Kundu, M.R., Gary, D.E.: 2000, *Astrophys. J.* **533**, 1053
Pryadko, J.M., Petrosian, V.: 1999, *Astrophys. J.* **515**, 873
Ramaty, R.: 1969, *Astrophys. J.* **158**, 753
Ramaty, R., Schwartz, R.A., Enome, S., Nakajima, H.: 1994, *Astrophys. J.* **436**, 941
Sakurai, T.: 1981, *Solar Phys.* **69**, 343
Sharma, R.R., Vlahos, L.: 1984, *Astrophys. J.* **280**, 405
Silva, A.V.R., Wang, H., Gary, D.E.: 2000, *Astrophys. J.* **545**, 1116
Simões, P.J.A., Costa, J.E.R.: 2003, *Bull. Astron. Soc. Braz.* **23**, 183
Simões, P.J.A., Costa, J.E.R.: 2006, *Astron. Astrophys.* **453**, 729
Staehli, M., Gary, D.E., Hurford, G.J.: 1989, *Solar Phys.* **120**, 351
Vlasov, V.G., Kuznetsov, A.A., Altyntsev, A.T.: 2002, *Astron. Astrophys.* **382**, 1061
Wang, H., Gary, D.E., Lim, J., Schwartz, R.A.: 1994, *Astrophys. J.* **433**, 379
Wiegelmann, T., Inhester, B.: 2003, *Solar Phys.* **214**, 287
Wu, C.S., Lee, L.C.: 1979, *Astrophys. J.* **230**, 621
Yokoyama, T., Nakajima, H., Shibasaki, K., Melnikov, V.F., Stepanov, A.V.: 2002, *Astrophys. J. Lett.* **576**, 87